IRSTI **30.19.19**

V. Kaliakin

University of Delaware, Newark, DE, U.S.A.
E-mail: kaliakin@udel.edu

Finite Element Investigation of Anisotropic Circular Plates

Abstract. The mathematical modeling and finite element analysis of solid circular plates, analyzed using continuum finite elements under conditions of axisymmetry, is investigated in this paper. Both isotropic and anisotropic material characterizations are considered. Once a suitable "baseline" model is developed, parametric analyses are performed so as to gain insight into the behavior of anisotropic solid circular plates.
Keywords: circular plates, anisotropy, transverse isotropy, axisymmetry, finite element method.

DOI: doi.org/10.32523/2616-7263-2023-142-1-7-22

1. Introduction

In structural mechanics, it is often possible to take advantage of the intrinsic structural behavior of a particular type of body to permit an *a priori* simplification of the spatial dependence of stress and deformation in the body. In this manner, it becomes possible to define and utilize effectively special theories of beams, cables, membranes, plates, shells, and so on. In each of these cases the geometric features of the body, together with the usual pattern of imposed loading, provide an opportunity to simplify the modeling process and to develop a model of lower spatial dimension.

A plate is a three-dimensional deformable body with two of the dimensions much greater than the third. Roughly speaking, a plate satisfies the requirement that $h << L$, where h is the thickness of the plate and L represents a characteristic dimension of the plate. By taking advantage of the fact that one characteristic dimension of the plate is much smaller than the other two, the general three-dimensional problem is reduced to a two-dimensional one.

General plate theories are commonly classified based on certain kinematic limitations related to the transverse displacement (w) of the plate. For example, in the "small" deflection theory of thin plates due to Lagrange, Poisson and Kirchhoff [6], $w << h$. In the "large" deflection theory of thin plates, the governing nonlinear partial differential equations are the so-called "Foppl - von Karman equations" [2, 5]. In this theory, w is approximately equal to h. The theory of moderately thick plates is due to Reissner [10] and Mindlin [8]. Finally, in membrane theory [2], $w >> h$.

The number of analytical (closed form) solutions available using such theories is somewhat limited, especially for plates employing an anisotropic material characterization. This is especially true for circular plates.

The use of numerical approaches such as the finite element and finite difference methods facilitates the analysis of plates in that such methods easily account for material inhomogeneity, variable plate thickness, anisotropic material idealizations, and so forth. Indeed, a plethora of specialized plate bending elements, having varying degrees of complexity, have been developed over the years for use in conjunction finite element analyses [13].

An alternative to such specialized elements are standard continuum elements. The use of such elements to mathematically model and simulate the behavior of plates has the advantage that no a priori assumptions regarding the associated kinematics need to be made. The plate is simply analyzed as an elastic body, with the kinematics dictated by the nature of the strain-displacement equations assumed in the formulation of the continuum elements. Finally, the level of material anisotropy characterizing the material is easily selected.

This paper investigates the mathematical modeling and finite element analysis of solid circular plates, analyzed using continuum finite elements under conditions of torsionless axisymmetry. Both isotropic and anisotropic material idealizations are considered. Once a suitable "baseline" model is developed, parametric analyses are performed on such plates with anisotropic material idealizations so as to gain insight into their behavior.

2. Background Information

Figure 1 shows a typical solid circular plate with outer radius equal to a and a thickness of h. Here r, θ, and z denote the radial, axial, and circumferential coordinates, respectively.

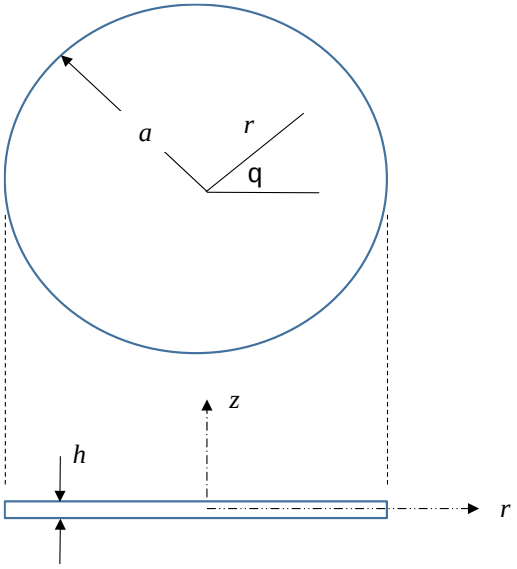

Figure 1. Schematic illustration of a solid circular plate in a cylindrical coordinate system

If the applied loading, the support conditions along the outer edge of the plate and the material idealization are independent of θ, the circular plate can be analyzed as a two-dimensional torsionless axisymmetric problem. The continuum elements suitable for the finite element analysis of such problems are thus triangles and quadrilaterals; the development of such elements follows a standard procedure [3].

3. Kinematic Relations

Assuming infinitesimal displacements and displacement gradients, the strain components, in cylindrical coordinates, associated with a torsionless axisymmetric analysis are

$$\varepsilon_{rr} = \frac{\partial u}{\partial r} \quad ; \quad \varepsilon_{zz} = \frac{\partial v}{\partial z} \quad ; \quad \varepsilon_{\theta\theta} = \frac{u}{r} \quad ; \quad \gamma_{rz} = \frac{\partial u}{\partial z} + \frac{\partial v}{\partial r} \tag{1}$$

where u and v denote the to the radial and axial displacements, respectively, and γ_{rz} denotes an "engineering" shear strain.

4. Constitutive Relations

Written in direct form, the general anisotropic elastic constitutive relations are written as $\boldsymbol{\varepsilon} = \mathbf{A}\boldsymbol{\sigma}$, where $\mathbf{A}$ is a symmetric compliance matrix, and

$$\boldsymbol{\varepsilon} = \left\{ \varepsilon_{rr} \quad \varepsilon_{zz} \quad \varepsilon_{\theta\theta} \quad \gamma_{rz} \right\}^T \quad ; \quad \boldsymbol{\sigma} = \left\{ \sigma_{rr} \quad \sigma_{zz} \quad \sigma_{\theta\theta} \quad \sigma_{rz} \right\}^T \tag{2}$$

where ε_{rr}, ε_{zz}, $\varepsilon_{\theta\theta}$ and $\gamma_{\rho z}$ are as defined in Equation (1) and σ_{rr}, σ_{zz}, $\sigma_{\theta\theta}$ and σ_{rz} are the corresponding stress components. In Equation (2), the superscript T denotes the operation of vector transposition.

Concerning material symmetries, a state of *general* anisotropy is not applicable for torsionless axisymmetric material idealizations, for conditions of axial symmetry cannot be maintained under such a state. A special case of anisotropy, consisting of a homogeneous, elastic transversely isotropic material bounded by one or more coaxial surfaces of revolution to give the axisymmetrically stratified material shown schematically in Figure 2 is, however, possible [7].

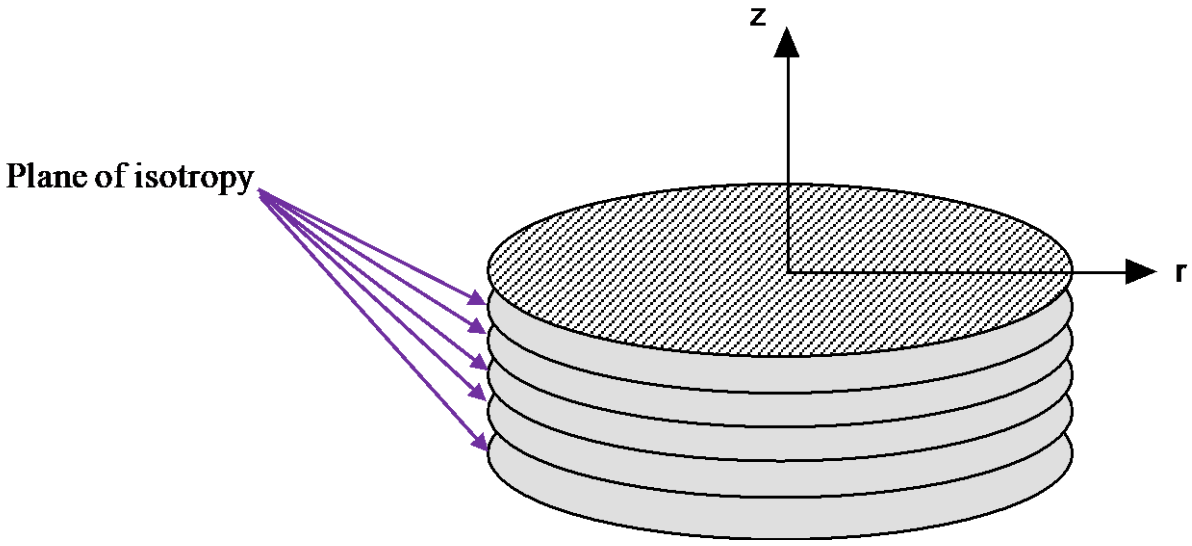

Figure 2. Schematic illustration of axisymmetrically stratified body

The associated compliance matrix is then

$$\mathbf{A} = \begin{bmatrix} 1/E_1 & -\nu_{21}/E_2 & -\nu_{31}/E_1 & 0 \\ -\nu_{12}/E_1 & 1/E_2 & -\nu_{32}/E_1 & 0 \\ -\nu_{13}/E_1 & -\nu_{23}/E_2 & 1/E_1 & 0 \\ 0 & 0 & 0 & 1/G_{12} \end{bmatrix} \tag{3}$$

Symmetry of $\mathbf{A}$ requires that

$$\frac{\nu_{21}}{E_2} = \frac{\nu_{12}}{E_1} \quad ; \quad \nu_{31} = \nu_{13} \quad ; \quad \frac{\nu_{32}}{E_1} = \frac{\nu_{23}}{E_2} \tag{4}$$

Thus, only *five* of the elastic constants entering the above equations are independent; i.e., E_1, E_2, ν_{12}, ν_{13}, and G_{12}. These constants are interpreted as follows [7]: E_1 is the elastic modulus for tension and

compression in the plane of isotropy, E_2 is the elastic modulus for tension and compression in a direction perpendicular to the plane of isotropy, ν_{12} is the Poisson's ratio characterizing contraction in a direction normal to the plane of isotropy resulting from tension in this plane, ν_{13} is the Poisson's ratio characterizing contraction in the plane of isotropy resulting from tension in the same plane, and G_{12} is the shear modulus for the perpendicular (radial) plane.

Using the infinitesimal strain-displacement relations given by Equation (1), along with the transversely isotropic constitutive relation given by Equation (3), two-dimensional continuum elements (i.e., triangles and quadrilaterals) suitable for torsionless axisymmetric analyses are developed following a standard procedure [3].

5. Development of Mathematical Models

The solid circular plate analyzed in this paper is assumed to have a radius of a = 1.50 m and a thickness of h = 0.075 m. The ratio of the thickness of the plate to its diameter is thus $h/2a$ = 0.025, which constitutes a "thin" plate [12]. The anisotropic material is assumed to be a T300/5208 carbon/epoxy composite that is characterized by the following values of the elastic constants [9]: E_1 = 1.090 x 10^7 kPa, E_2 = 1.530 x 10^8 kPa, ν_{12} = 0.0210, ν_{13} = 0.0214 and G_{12} = 5.600 x 10^6 kPa. All analyses described in this paper were performed using the APES+ computer program [4].

Before analyzing the circular plate, it is necessary to determine a mesh that is suitably fine so as to give accurate results. For this purpose, the plate material is assumed to be isotropic linear elastic with an elastic modulus E = 8.195 x 10^7 kPa (an average of E_1 and E_2) and a Poisson's ratio of ν = 0.30.

The plate is loaded by a uniformly distributed load of q = 6.0 kPa. To properly account for conditions along the axis of symmetry (i.e., r = 0), the nodal constraint u = 0 must be specified at all nodes along this axis. Along its outer edge, the plate is assumed to be simply supported. To account for this edge condition, at the point (r, z) = (a, 0), u = v = 0 is specified. Figure 3 shows the mathematical model used in the finite element analyses of the uniformly loaded, simply supported solid circular plate.

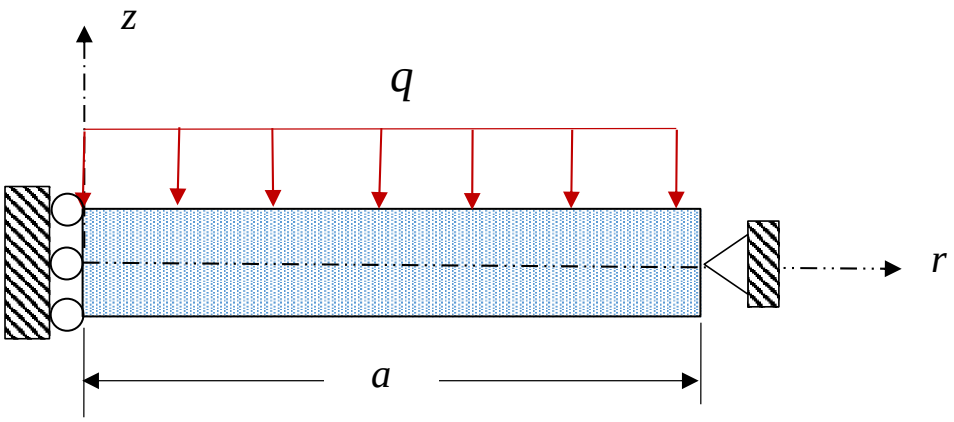

Figure 3. Mathematical model of uniformly loaded, simply supported solid circular plate

According to the Lagrange-Poisson-Kirchhoff thin plate theory, the transverse displacement of this plate is given by [12]

$$v(r) = -\frac{q\left(a^2 - r^2\right)}{64D}\left[\left(\frac{5+\nu}{1+\nu}\right)a^2 - r^2\right] \tag{5}$$

where $D = Eh^3 / 12(1 - \nu^2)$.

The plate is first discretized using bi-linear, 4-node quadrilateral (Q4) elements. The first mesh consists of two elements in the *z*-direction by five elements in the *r*-direction. Figure 4 plots the approximate transverse displacement along the *r*-axis, normalized by the value given by Equation (5), versus the radial distance (*r*) along the plate normalized by the radius *a*. As evident from this figure, the 2 by 5 mesh of Q4 elements (31 unconstrained displacement degrees of freedom) significantly underpredicts the transverse displacement of the plate. Stated in another way, the 2 by 5 mesh of Q4 elements is *too stiff*.

The mesh is next refined by doubling the number of elements in both the *z* and *r*-directions. The results of this 4 by 10 mesh of Q4 elements (103 unconstrained displacement degrees of freedom) are also plotted in Figure 4. Although these results are more accurate than for the 2 by 5 mesh, they are still only about 84% of the thin plate solution given by Equation (5). Continued mesh refinement to an 8 by 20 mesh (367 unconstrained displacement degrees of freedom) and then a 16 by 40 mesh (1375 unconstrained displacement degrees of freedom) finally gives approximate transverse displacements that are equal to the thin plate solution (see Figure 4).

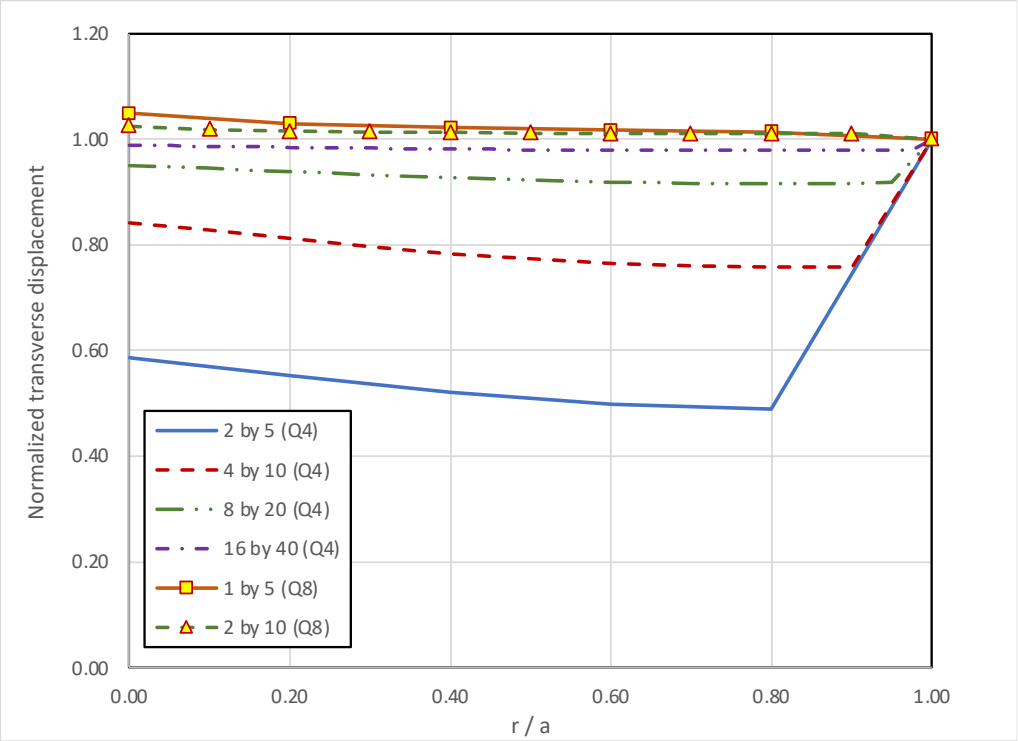

Figure 4. Summary of mesh sensitivity study for a uniformly loaded, simply supported, isotropic elastic thin solid circular plate

The plate is next discretized using bi-quadratic, 8-node quadrilateral (Q8) elements. The first mesh consists of one element in the *z*-direction by 5 elements in the *r*-direction (51 unconstrained displacement degrees of freedom). As evident from Figure 4, the approximate solution is very close to the thin plate solution. Since the latter solution neglects shear deformations but the continuum elements include such deformations, convergence to a normalized transverse displacement slightly in excess of unity (1.00) is to be expected. This observation is supported by the results of a 2 by 10 mesh of Q8 elements (143 unconstrained displacement degrees of freedom), which are also plotted in Figure 4.

Based on the results shown in Figure 4, it is evident that the performance of the Q8 elements is significantly more efficient than for the Q4 elements. This observation is consistent with similar findings made in beam bending simulations [1]. Consequently, in all subsequent analyses of solid circular plates made in this paper, the 2 by 10 mesh of Q8 elements constitutes the "baseline" mesh.

6. Parametric Analysis of a Thin Anisotropic Solid Circular Plate

The uniformly loaded, simply supported solid circular plate whose mathematical model is shown in Figure 3 is next assumed to be made of the T300/5208 carbon/epoxy composite that is characterized using the model parameter values given in Section 5.

A series of parametric analyses of this plate was performed to gain insight into the behavior of a solid circular plate that is characterized by the aforementioned transversely isotropic material idealization. In each such analysis, one parameter value is varied while all other aspects of the mathematical model are unchanged from the "baseline" values given in Section 5. These "baseline" values of the model parameters give the following ratios: $n = E_1/E_2 = 0.071$, $m = \nu_{12}/\nu_{13} = 0.981$, and $p = G_{12}/E_2 = 0.037$.

The 2 by 10 mesh of bi-quadratic 8-node quadrilateral (Q8) elements, which was verified for accuracy in Section 5, is used in all the parametric analyses.

6.1 Effect of Variations in E_1

In the first set of parametric analyses, the value of $n = E_1/E_2$ is increased from the "baseline" value of 0.071 to 1.0, 5.0 and then to 10.0. These values are obtained by keeping the value of E_2 constant and suitably increasing the value of E_1. Figure 5 shows the variation of the radial stress (σ_{rr}) with normalized depth ($2z/h$) as a function of n near the mid-span of the plate (i.e., for r approximately equal to $a/2$). As evident from this figure, variations in n have very little effect on the simulated radial stress distribution.

Figure 6 shows the variation of the circumferential stress ($\sigma_{\theta\theta}$) with normalized depth ($2z/h$) as a function of n near the mid-span of the plate. As evident from this figure, variations in n have essentially no effect on the simulated circumferential stress distribution, which remains linear through the depth of the plate.

To better understand the results shown in Figures 5 and 6, consider the radial and circumferential stress distributions associated with a uniformly loaded, simply supported solid circular plate that is characterized as an *isotropic* elastic material; viz., [12]

$$\sigma_{rr} = -\frac{3\bar{q}z}{4h^3}(3+\nu)(a^2-r^2) \quad ; \quad \sigma_{\theta\theta} = -\frac{3\bar{q}z}{4h^3}\left[a^2(3+\nu) - r^2(1+3\nu)\right] \tag{6}$$

From Equations (6) it is evident that, for a given value of Poisson's ratio (ν), the radial and circumferential stress distributions are independent of the elastic modulus (E). In a similar manner, for the present transversely isotropic material idealization, increases in the value of E_1 have negligible effects on the radial and circumferential stress distributions.

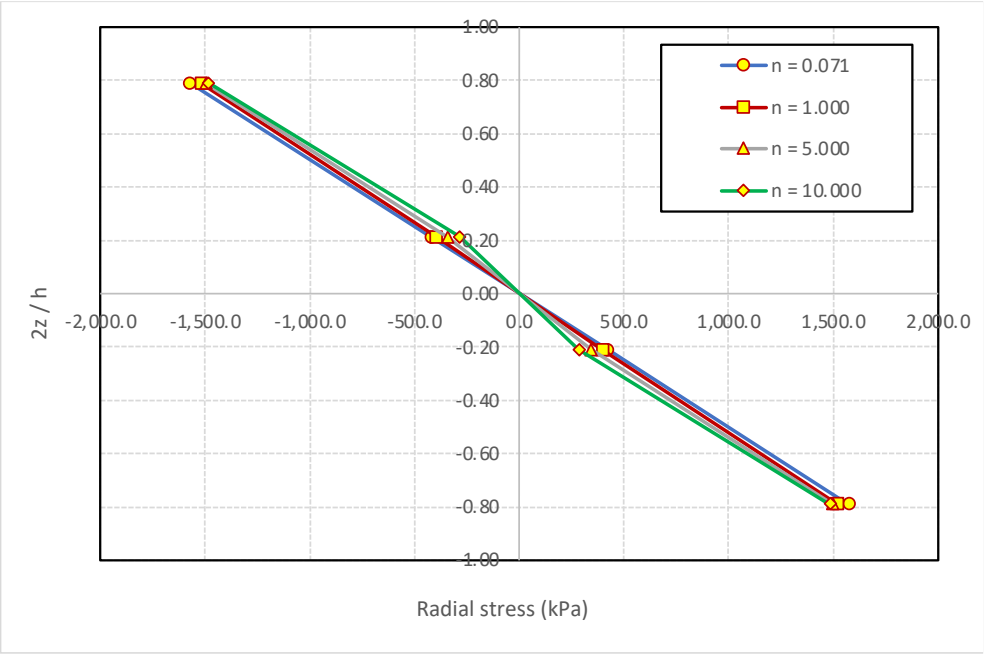

Figure 5. Effect of variations in $n = E_1/E_2$ on the simulated radial stress distribution through the depth of a solid circular plate

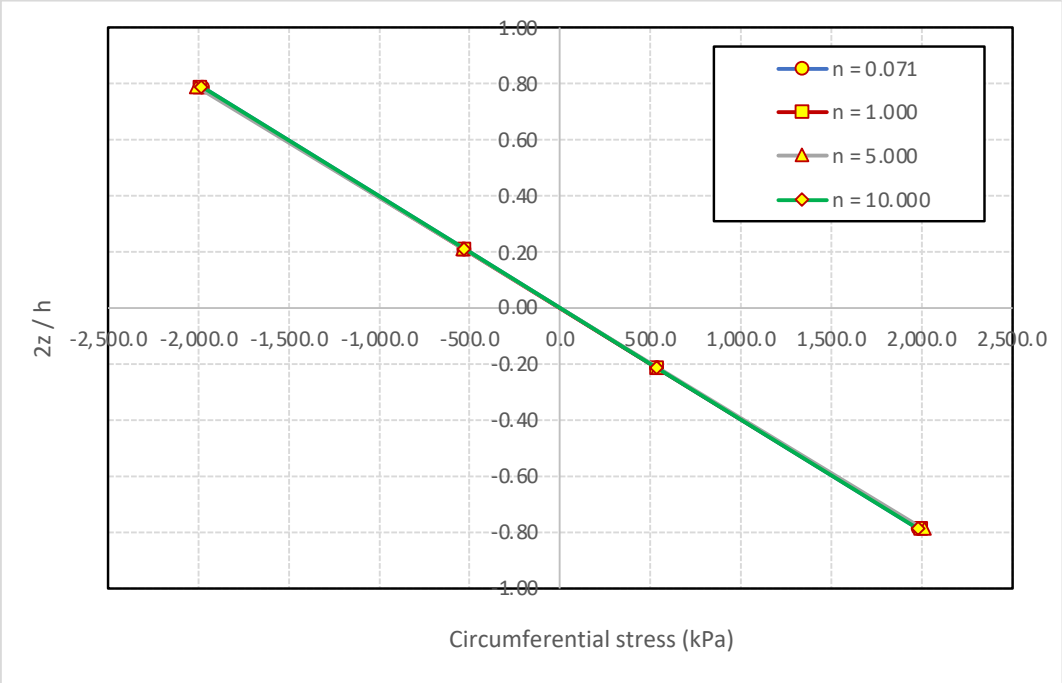

Figure 6. Effect of variations in $n = E_1/E_2$ on the simulated circumferential stress distribution through the depth of a solid circular plate

Figure 7 shows the variation of the axial stress (σ_{zz}) with normalized depth ($2z/h$) as a function of n near the mid-span of the plate. As evident from this figure, variations in n have a rather pronounced effect on the simulated σ_{zz} distribution. In particular, for $n = 0.071$, the axial stress changes sign with depth from positive (tensile) to negative (compressive). For higher values of n, σ_{zz} remains negative (i.e., compressive) throughout the depth and the magnitude of this stress is significantly lower than for $n = 0.071$.

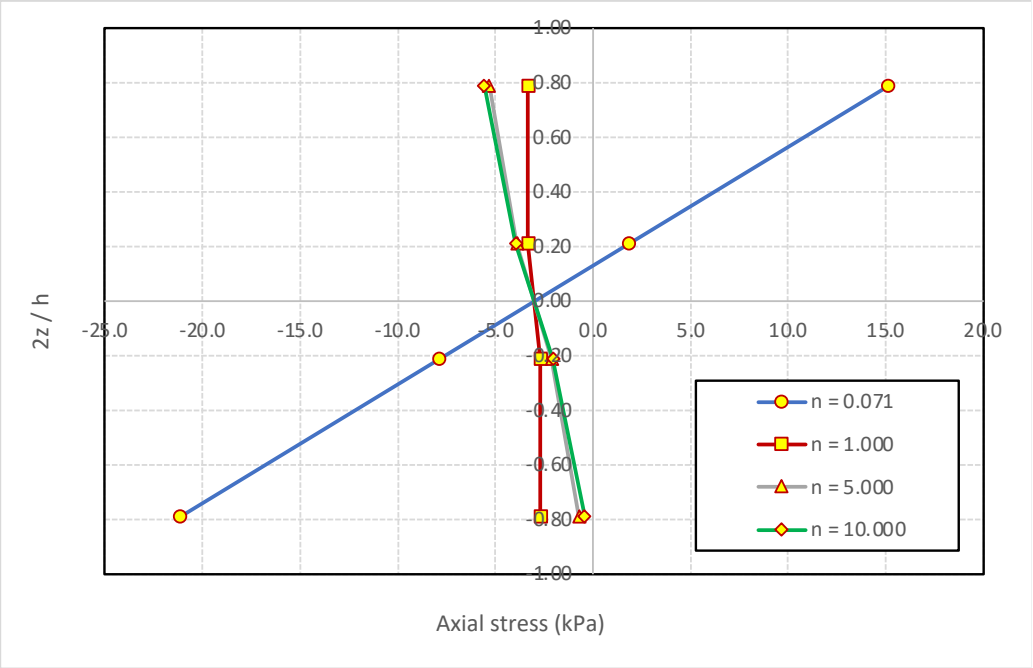

Figure 7. Effect of variations in $n = E_1/E_2$ on the simulated axial stress distribution through the depth of a solid circular plate

6.2 Effect of Variations in ν_{12}

In the second set of parametric analyses, the value of $m = \nu_{12}/\nu_{13}$ is varied from the "baseline" value of 0.981. In particular, values of $m = 0.100$ and 5.000 compliment this "baseline" value. These values are obtained by keeping the value of ν_{13} constant and suitably varying the value of ν_{12}.

Variations in m do not affect the radial, circumferential and shear stress distributions; the figures showing the simulated stresses are thus omitted for brevity. By contrast, as evident from Figure 8, changes in m have a pronounced effect on the axial stress distribution near the mid-span of the plate. In particular, for a value of $m = 0.100$, σ_{zz} is purely negative (i.e., compressive). Increases in m cause the axial stress distribution through the depth to change sign and to increase in magnitude.

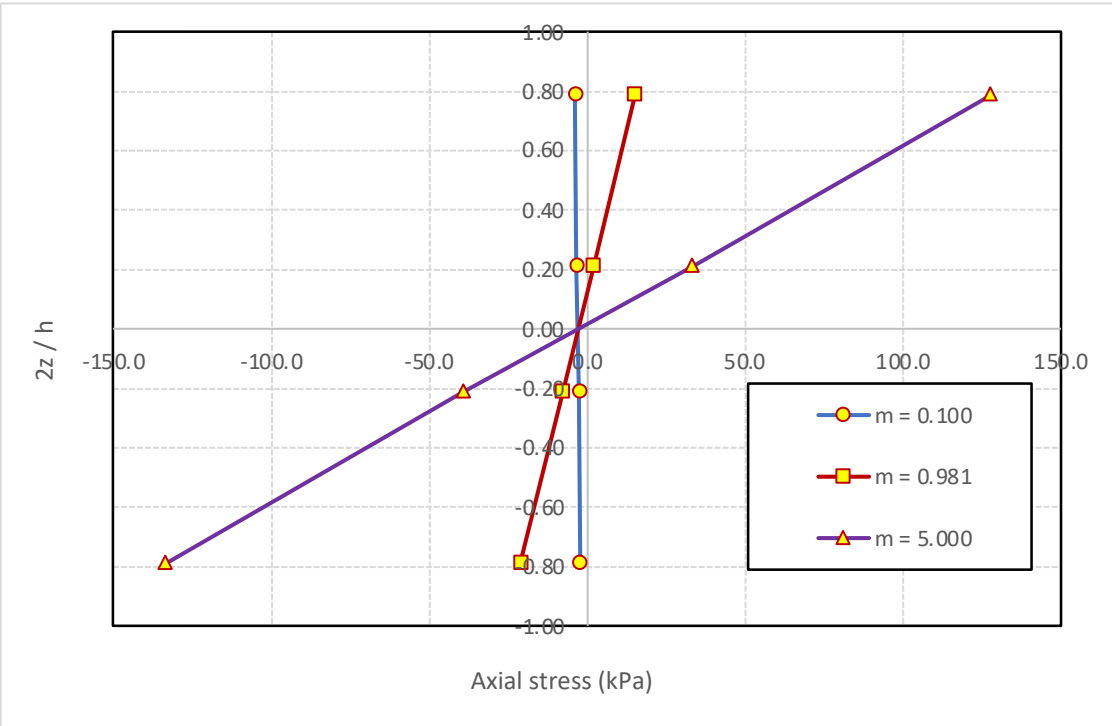

Figure 8. Effect of variations in $m = \nu_{12}/\nu_{13}$ on the simulated axial stress distribution through the depth of a solid circular plate

6.3 Effect of Variations in G_{12}

In the final set of parametric analyses, the value of $p = G_{12}/E_2$ is varied from the "baseline" value of 0.037. In particular, values of $p = 0.250$ and 1.000 compliment this "baseline" value. These values of p are obtained by keeping the value of E_2 constant and suitably increasing the value of G_{12}.

Variations in p do not affect the radial and circumferential stress distributions; the figures showing the simulated stresses are thus omitted for brevity. As evident from Figure 9, variations in p do affect the σ_{zz} distribution in the plate. In particular, increases in p cause the axial stress distribution to change sign in the top and bottom halves of the cross-section.

Increases in p (and thus G_{12}) stiffen the shear response in the r-z plane. Consequently, the shear strains and shear stresses (σ_{rz}) will be reduced. This trend is confirmed by Figure 10.

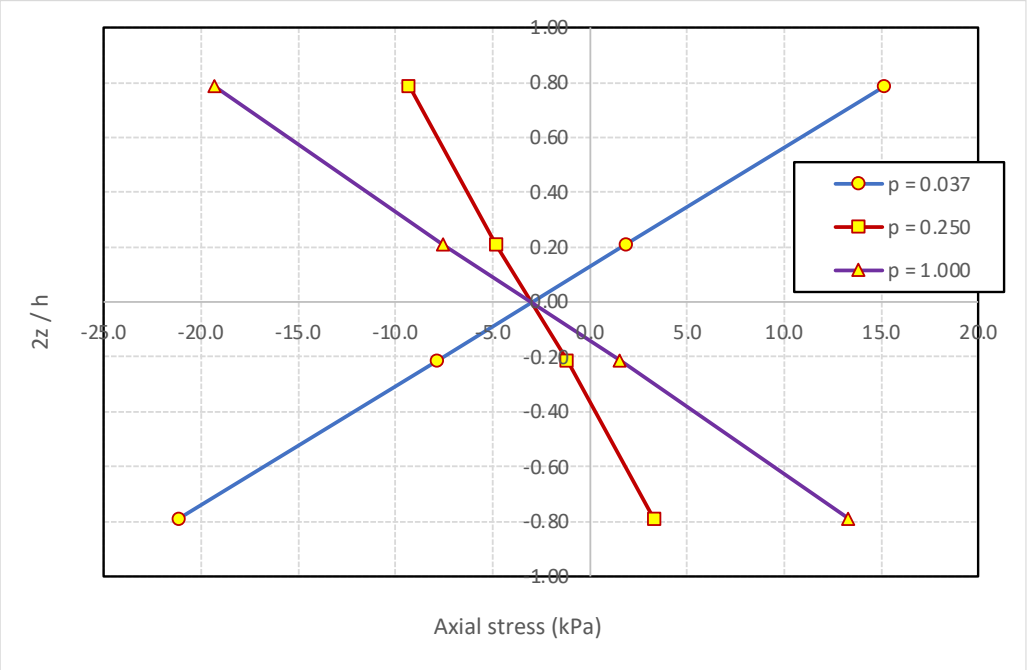

Figure 9. Effect of variations in $p = G_{12}/E_2$ on the simulated axial stress distribution through the depth of a solid circular plate

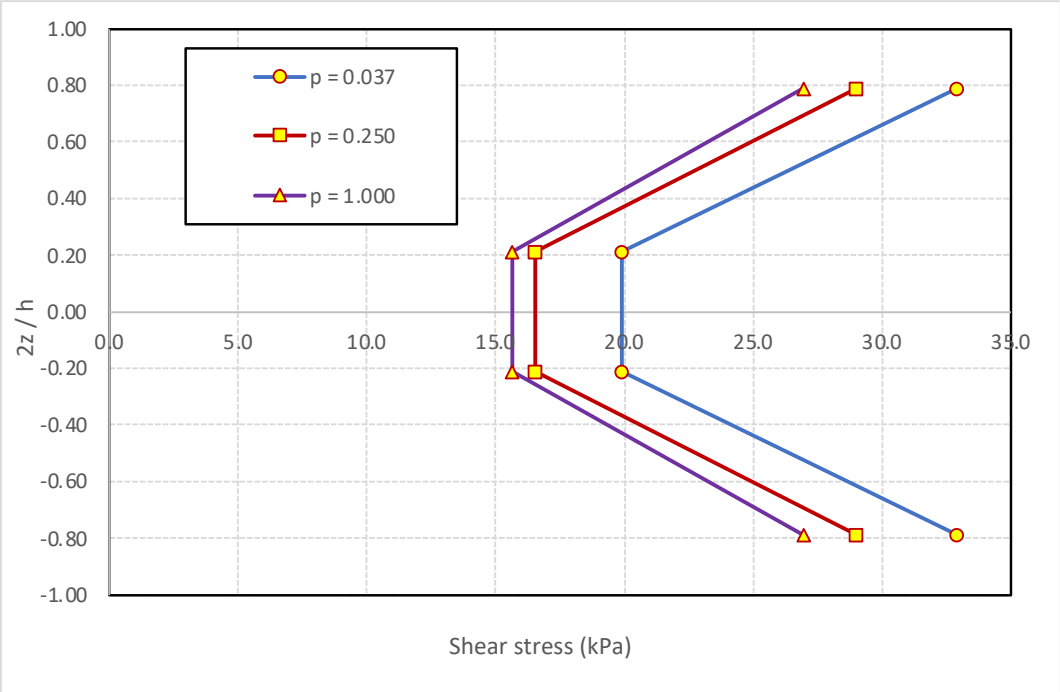

Figure 10. Effect of variations in $p = G_{12}/E_2$ on the simulated shear stress distribution through the depth of a solid circular plate

7. Parametric Analysis of a Thick Anisotropic Solid Circular Plate

Specialized structural plate bending theories typically have restrictions regarding the thickness of the plate. For example, the Lagrange-Poisson- Kirchhoff thin plate theory is restricted to very thin plates [12]. The Reissner-Mindlin theory [10, 8], on the other hand, is applicable to moderately thick plates.

One of the benefits of analyzing plates using continuum elements is that there are no restrictions placed on the thickness of the plate, provided that the strains in the plate remain infinitesimal (recall the discussion of kinematic relations given in Section 3).

To investigate the effect that variations in thickness have on the simulated bending response of a solid circular plate, the plate having a radius of a = 1.50 m is again analyzed. Instead of the simply supported edge considered in Sections 5 and 6, the outer edge of the plate is now assumed to be clamped. The constraint $u = v = 0.0$ is thus specified at all nodes located on the boundary $r = a$.

The plate is idealized as a transversely isotropic material; the values of the associated material parameters are as given in Section 5.

A concentrated force (P) that is statically equivalent to the total force associated with the uniformly distributed force per unit area (q) is applied at the center of the plate. That is, $P = q(\pi a^2)$ = (6.0 kPa)(π)(1.50 m)^2 = 42.4 kN. Figure 11 shows the mathematical model used in the finite element analyses of the clamped solid circular plate subjected to a concentrated force applied at the center of the plate.

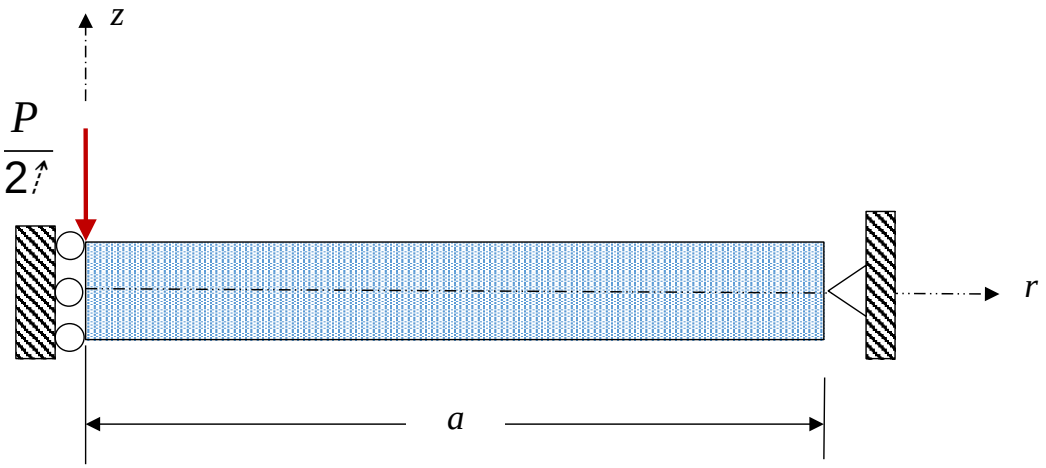

Figure 11: Mathematical model of clamped solid circular plate subjected to a concentrated force applied at the center of the plate

The thickness of the plate (h) is next varied. In particular, h is first assumed to equal to 0.300 m. The thickness to diameter ratio ($h/2a$) is thus 0.100, which corresponds to a thin plate. To maintain the same sized elements through the thickness of the solid circular plate, an 8 by 10 mesh of Q8 elements is used to discretize the plate. The plate thickness is next increased to 0.600 m. Now $h/2a$ = 0.200, which corresponds to a moderately thick plate. For consistency, a 16 by 10 mesh of Q8 elements is used to discretize the plate. Finally, the plate thickness is increased to 0.600 m. Now $h/2a$ = 0.400, which corresponds to a thick plate. For consistency, a 32 by 10 mesh of Q8 elements is used to discretize the plate.

Figure 12 shows the variation of σ_{rr} with normalized depth ($2z/h$) as a function of h near the mid-span of the plate. As evident from this figure, increases in h cause the distribution of σ_{rr} to deviate from linearity. This phenomenon is similar to the variation of the normal stress distribution observed in deep beams [11]. Since more material is present in plates with increased thickness (for the same applied force), the magnitude of σ_{rr} decreases with increases in h.

Figure 13 shows the variation of $\sigma_{\theta\theta}$ with normalized depth as a function of h near the mid-span of the plate. Similar to the σ_{rr} distribution, linearity of $\sigma_{\theta\theta}$ is lost with increases in h. also similar to the case of σ_{rr}, the magnitude of $\sigma_{\theta\theta}$ decreases with increases in plate thickness.

The variation of the axial stress distribution with normalized depth as a function of h is very similar to the σ_{rr} distribution shown in Figure 13. Consequently, the figure showing the simulated σ_{zz} values is thus omitted for brevity.

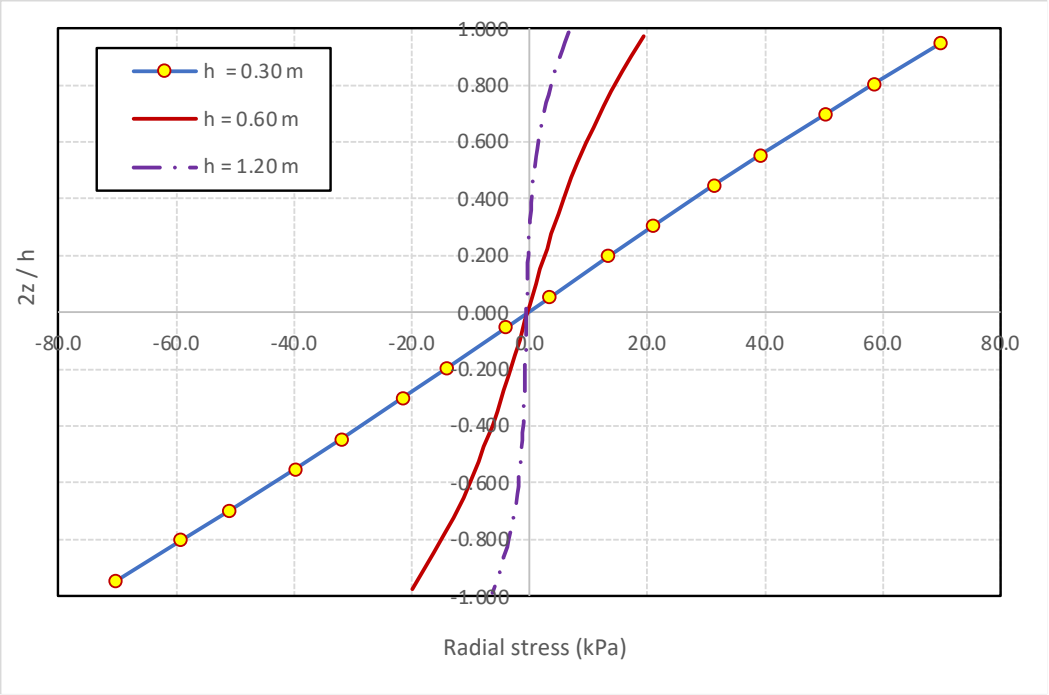

Figure 12. Effect of variations in plate thickness (*h*) on the simulated radial stress distribution through the depth of a transversely isotropic solid circular plate

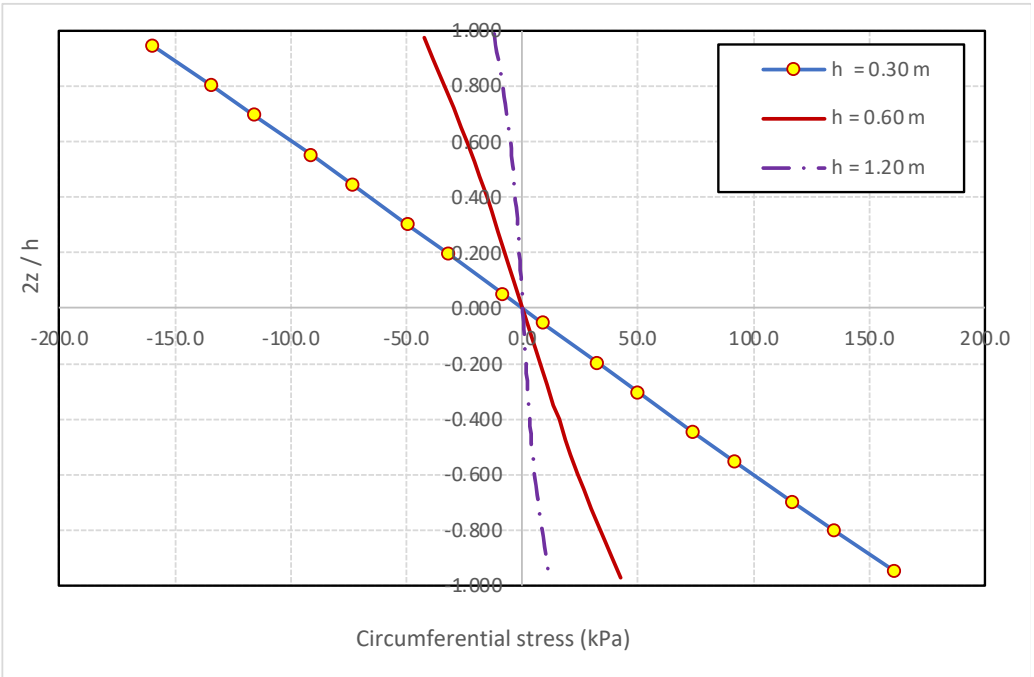

Figure 13. Effect of variations in plate thickness (*h*) on the simulated circumferential stress distribution through the depth of a transversely isotropic solid circular plate

Figure 14 shows the variation of σ_{rz} with normalized depth as a function of h near the mid-span of the plate. As evident from this figure, the parabolic distribution of σ_{rz} is largely maintained with increasing values of h. Similar to the σ_{rr} and $\sigma_{\theta\theta}$ distributions, the magnitude of σ_{rz} decreases with increases in h as there is more material available to support the same magnitude of P.

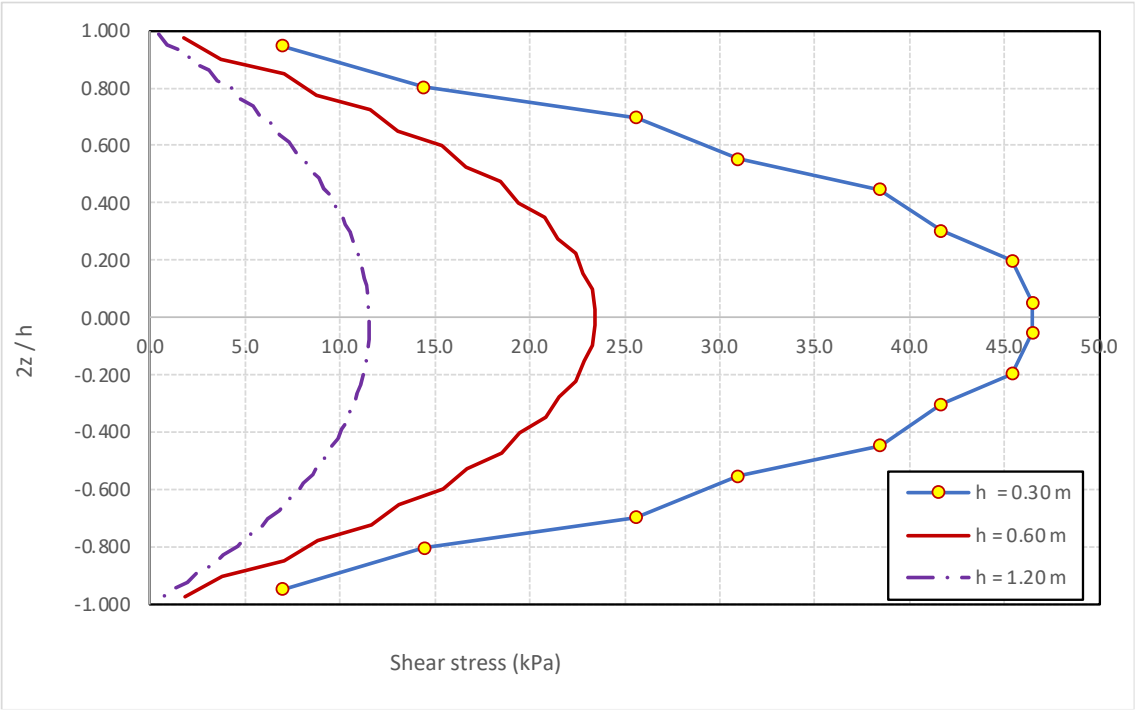

Figure 14. Effect of variations in plate thickness (*h*) on the simulated shear stress distribution through the depth of a transversely isotropic solid circular plate

8. Conclusions

The mathematical modeling and torsionless axisymmetric finite element analysis of solid circular plates with isotropic and anisotropic material idealizations was described in this paper. Once a suitable "baseline" model was developed, parametric analyses were performed on the plate so as to gain insight into the behavior of anisotropic circular plates. Based on the results of the aforementioned analyses, the following conclusions were reached.

In simulating the bending of circular plates using continuum elements, the performance of quadratic quadrilateral elements was superior to that of linear elements. This is consistent with beam bending simulations, where linear elements are known to exhibit fictitious ("parasitic") shear deformations that stiffen the simulated response [1].

When simulating the response of a transversely isotropic solid circular plate, variations in the ratio $n = E_1/E_2$ had essentially no effect on the radial and circumferential stress distributions. Increases in n did, however, cause the axial stress to transition from a linear distribution that changed sign with depth from positive (tensile) to negative (compressive) to a distribution that was purely compressive.

Variations in $m = \nu_{12}/\nu_{13}$ did not affect the radial, circumferential and shear stress distributions. Changes in m did have a pronounced effect on the axial stress distribution. In particular, for a value of m = 0.100, the axial stress is purely negative (i.e., compressive). Increases in m caused the axial stress distribution through the depth to change sign and to increase in magnitude.

Variations in $p = G_{12}/E_2$ did not affect the radial or circumferential stress distributions. Increases in p did affect the axial stress distribution, causing the axial stress distribution to change sign in the top and bottom halves of the cross-section. Increases in p also stiffen the plate's shear response in the r-z plane, causing the magnitude of the shear strain and shear stress to reduce.

Increases in the plate thickness cause the radial and circumferential stress distributions to become nonlinear through the depth of a transversely isotropic solid circular plate. This is consistent with the distribution of normal stresses in a deep beam [11]. The magnitude of the radial and circumferential stresses decreases with increasing plate thickness.

Increases in plate thickness do not affect the parabolic distribution with depth of the shear stress. Similar to the radial and circumferential stress distributions, the magnitude of the shear stress decreases with increasing plate thickness.

Acknowledgments

A portion of this paper was written while the author was a Visiting Foreign Professor at the L. N. Gumilyov Eurasian National University in Astana, Kazakhstan.

References

1. Concepts and Applications of Finite Element Analysis / R. D. Cook, D. S. Malkus, M. F. Plesha, R. J. Witt, R. J. | 4th edition | New York: John Wiley and Sons, 2002.
2. Vorlesungen uber technische Mechanik / A. Foppl | Leipzig: B. G. Teubner, 1907.
3. Approximate Solution Techniques, Numerical Modeling and Finite Element Methods / V. N. Kaliakin | New York: Marcel Dekker, Inc., 2001.
4. APES+ (Analysis Program for Earth Structures) Computer Program Documentation, User Manual / V. N. Kaliakin // University of Delaware, Department of Civil Engineering, Newark, DE, 2022 – Mode of access: http://nwp.engr.udel.edu/cieg/faculty/kaliakin/apes_doc.pdf
5. Festigkeitsproblem im Maschinenbau / T. von Karman // Encyk. der mathematik Wiss. 1910 – Vol. IV. – P. 348–351.
6. Uber das Gleichgewicht und die Bewegung einer elastishen scheibe / G. Kirchhoff // Journel fur die reine und angewandte mathematic. 1850 – Vol. 40 – P. 51–88.
7. Theory of Elasticity of an Anisotropic Body / S. G. Lekhnitskii | Moscow: Mir Publishers, 1981.
8. Influence of rotary inertia and shear on flexural motions of isotropic elastic plates / R. D. Mindlin // Journal of Applied Mechanics. 1951. Vol. 18. No. 1. – P. 31–38.
9. Analysis of Cylindrical Composite Shells / E. C. Preissner // PhD Dissertation. Department of Mechanical Engineering, University of Delaware, 2002.
10. The effect of transverse shear deformation on the bending of elastic plates / E. Reissner // Journal of Applied Mechanics. 1945. Vol. 12. No. 2-P. 69–77.
11. Theory of Elasticity / S. P. Timoshenko, J. N. Goodier | 3rd edition | New York: McGraw-Hill, 1970.
12. Theory of Plates and Shells / S. P. Timoshenko, S. Woinowsky-Krieger | 2nd edition | New Yoprk: McGraw-Hill Book Co., 1959.
13. The Finite Element Method / O. C. Zienkiewicz, R. L. Taylor | 5th Edition | Volume 2: Solid Mechanics | Oxford: Butterworth Heinemann, 2000.

В.Н. Калякин

Делавэр университеті, Ньюарк, Делавэр, АҚШ

Анизотропты дөңгелек пластиналарды шекті элементтермен зерттеу

Аңдатпа. Бұл мақалада осьтік симметрия жағдайында шекті элементтерін қолдану арқылы талданған тұтас дөңгелек пластиналарды математикалық модельдеу және шекті элементтермен талдау зерттеледі. Изотропты және анизотропты материалды сипаттау қарастырылады. Сәйкес «базалық» модель әзірленгеннен кейін, анизотропты қатты дөңгелек пластиналардың тәртібін түсіну үшін параметрлік талдаулар орындалады.

Түйін сөздер: дөңгелек пластиналар, анизотропия, көлденең изотропия, осьтік симметрия, шекті элементтер әдісі.

В.Н. Калякин

Делавэрский университет, Ньюарк, Делавэр, США

Исследование методом конечных элементов анизотропных круглых пластин

Аннотация. В статье исследуется математическое моделирование и анализ методом конечных элементов сплошных круглых пластин, анализируемых с использованием сплошных конечных элементов в условиях осевой симметрии. Рассматриваются как изотропные, так и анизотропные характеристики материала. После разработки подходящей «базовой» модели выполняется параметрический анализ, чтобы получить представление о поведении анизотропных сплошных круглых пластин.

Ключевые слова: круглые пластины, анизотропия, поперечная изотропия, осесимметрия, метод конечных элементов.

References

1. Concepts and Applications of Finite Element Analysis / R. D. Cook, D. S. Malkus, M. F. Plesha, R. J. Witt, R. J. | 4th edition | New York: John Wiley and Sons, 2002.
2. Vorlesungen uber technische Mechanik / A. Foppl | Leipzig: B. G. Teubner, 1907.
3. Approximate Solution Techniques, Numerical Modeling and Finite Element Methods / V. N. Kaliakin | New York: Marcel Dekker, Inc., 2001.
4. APES+ (Analysis Program for Earth Structures) Computer Program Documentation, User Manual / V. N. Kaliakin // University of Delaware, Department of Civil Engineering, Newark, DE, 2022 – Mode of access: http://nwp.engr.udel.edu/cieg/faculty/kaliakin/apes_doc.pdf
5. Festigkeitsproblem im Maschinenbau / T. von Karman // Encyk. der mathematik Wiss. 1910 – Vol. IV. – P. 348–351.
6. Uber das Gleichgewicht und die Bewegung einer elastishen scheibe / G. Kirchhoff // Journel fur die reine und angewandte mathematic. 1850 – Vol. 40 – P. 51–88.
7. Theory of Elasticity of an Anisotropic Body / S. G. Lekhnitskii | Moscow: Mir Publishers, 1981.
8. Influence of rotary inertia and shear on flexural motions of isotropic elastic plates / R. D. Mindlin // Journal of Applied Mechanics. 1951. Vol. 18. No. 1. – P. 31–38.
9. Analysis of Cylindrical Composite Shells / E. C. Preissner // PhD Dissertation. Department of Mechanical Engineering, University of Delaware, 2002.
10. The effect of transverse shear deformation on the bending of elastic plates / E. Reissner // Journal of Applied Mechanics. 1945. Vol. 12. No. 2 – P. 69–77.
11. Theory of Elasticity / S. P. Timoshenko, J. N. Goodier | 3rd edition | New York: McGraw-Hill, 1970.
12. Theory of Plates and Shells / S. P. Timoshenko, S. Woinowsky-Krieger | 2nd edition | New Yoprk: McGraw-Hill Book Co., 1959.
13. The Finite Element Method / O. C. Zienkiewicz, R. L. Taylor | 5th Edition | Volume 2: Solid Mechanics | Oxford: Butterworth Heinemann, 2000.

Information about author:

В.Н. Калякин – PhD, профессор, кафедра гражданской и экологической инженерии, Делавэрский университет, Ньюарк, Делавэр, США.

В.Н. Калякин – PhD, профессор, азаматтық және инженерлік экология кафедрасы, Делавэр университеті, Ньюарк, Делавэр, АҚШ.

V. Kaliakin – PhD, Professor, Department of Civil & Environmental Engineering, University of Delaware, Newark, Delaware, U.S.A.